Journal of Biomedical Materials Research Part B: Applied Biomaterials

WILEY

Semi-interpenetrating polymer network cryogels based on poly(ethylene glycol) diacrylate and collagen as potential off-the-shelf platforms for cancer cell research

SCHOLARONE™
Manuscripts

Semi-interpenetrating polymer network cryogels based on poly(ethylene glycol) diacrylate and collagen as potential off-the-shelf platforms for cancer cell research

Ugo Masullo[1], Anna Cavallo[1], Maria Raffaella Greco[2], Stephan J. Reshkin[2], Maria Mastrodonato[3], Nunzia Gallo[1], Luca Salvatore[1], Tiziano Verri[4], Alessandro Sannino[1], Rosa Angela Cardone[2], Marta Madaghiele[1*]

[1]Department of Engineering for Innovation, University of Salento, Via per Monteroni, 73100 Lecce, Italy

[2]Department of Bioscience, Biotechnologies and Biopharmaceutics, University of Bari, Via Orabona 4, 70125 Bari, Italy

[3]Department of Biology, University of Bari, Via Orabona 4, 70125 Bari, Italy

[4]Department of Biological and Environmental Sciences and Technologies, University of Salento, Via per Monteroni, 73100 Lecce, Italy

*Corresponding author:

Marta Madaghiele

Department of Engineering for Innovation

University of Salento

Via per Monteroni, 73100 Lecce, Italy

e-mail: marta.madaghiele@unisalento.it

Phone: +39 0832 297236

DECLARATIONS OF INTEREST: None

ABSTRACT

In the present work, we investigated the potential of novel semi-interpenetrating polymer network (semi-IPN) cryogels, obtained through ultraviolet exposure of aqueous mixtures of poly(ethylene glycol) diacrylate and type I collagen, as tunable off-the-shelf platforms for 3D cancer cell research. We synthesized semi-IPN cryogels with variable collagen amounts (0.1% and 1% w/v) and assessed the effect of collagen on key cryogel properties for cell culture, e.g. porosity, degradation rate and mechanical stiffness. Then, we investigated the ability of the cryogels to sustain the long-term growth of two pancreatic ductal adenocarcinoma (PDAC) cell populations, the parenchymal Panc1 cells and their derived cancer stem cells. Results revealed that both cell lines efficiently infiltrated, attached and expanded in the cryogels over a period of 14 days. However, only when grown in the cryogels with the highest collagen concentration, both cell lines reproduced their characteristic growth pattern previously observed in collagen-enriched organotypic cultures, biomimetic of the highly fibrotic PDAC stroma. Cellular pre-embedding in Matrigel, i.e. the classical approach to develop/grow organoids, interfered with an efficient intra-scaffold migration and growth. Although preliminary, these findings highlight the potential of the proposed cryogels as reproducible and tunable cancer cell research platforms.

KEYWORDS

Poly(ethylene glycol) diacrylate, cryogels, porosity, 3D organotypic culture, cancer cell research

1. INTRODUCTION

Interpenetrating polymer networks (IPNs) are composite systems formed by two (or more) polymer networks that are independently crosslinked but highly intertwined, being one network created in the presence of the other.[1] Binary systems where a polymer network is formed around un-crosslinked chains of a second polymer are defined as semi-IPNs.[2-6]

With focus on biomedical applications, IPN and semi-IPN hydrogels are highly attractive for the design of biocompatible and biomimetic matrices that typically combine the advantages of synthetic polymers (e.g. easily tunable properties, high mechanical strength) with those of extracellular matrix (ECM) or natural macromolecules (e.g. presence of cell-interactive domains, degradability).[1-9] Not surprisingly, poly(ethylene glycol) (PEG) and its derivatives have emerged as ideal platforms for the design of tunable cell-instructive hydrogels. This is due to the intrinsic resistance of PEG to protein adsorption, which hinders non-specific cell-material interactions, as well as the versatility of PEG to be functionalized with multiple ECM molecules or moieties.[10-14] Therefore, in the last two decades various ECM-mimicking PEG-based hydrogels, including peptide-functionalized hydrogels,[10,11] IPNs[7,8,14] and semi-IPNs,[2-6] have been proposed to control cell behavior and stimulate tissue regeneration, for *in vitro* and *in vivo* use.

However, one of the main limitations of hydrogels in tissue engineering is represented by their small mesh size (up to a few tens of nanometers[15]), which may hamper a homogeneous cell infiltration in the whole hydrogel volume and/or impede a prompt nutrient supply to cells that are located in the inner regions of the hydrogel. Macroporous hydrogel networks, suitable for efficient 3D cell infiltration and culture, may be obtained by several techniques,[16-18] including cryogelation.

Cryogels are recognized as an important progress for 3D culture systems, due to their unique combination of elevated hydration and interconnected macro-porosity with high stiffness and toughness.[19] Cryogels are indeed obtained by gelation of polymer/monomer precursor solutions at sub-zero temperatures, so that the crosslinking reaction takes place only in the semi-liquid phases located among ice crystals, where the polymer/monomer concentration is locally increased. As such, the resulting polymer networks display not only high porosity but also robust pore walls, which provide them with enhanced mechanical properties and strong shape memory, over both non-porous hydrogels and other types of porous hydrogels.

Along with their use as scaffolds for tissue regeneration,[18,20-22] cryogels are also being increasingly explored to develop 3D functional tumor models *in vitro*.[23-26] Since cancer cell growth is modulated by the stiffness of the surrounding matrix, with cancerous tissues being generally stiffer than non-malignant tissues,[23,27] cryogels may indeed be useful to mimic the strength and the elasticity of tumors, thus allowing to analyze the biomechanical cues involved in cell-matrix interactions and pathogenesis. While animal tumor models typically show poorly predictive results,[28] 2D cancer cell cultures are insufficient to recapitulate the complex 3D structure of tumors and the underlying crosstalk between cancer cells and their ECM, which is known to guide cancer progression and metastasis.[29,30] Therefore, there is an increasing need to develop 3D *in vitro* tumor niches able to more closely mimic the pathological microenvironment *in vivo*.[31] Various 3D culture platforms for cancer cells have been proposed so far.[32-34] Starting from the hanging drop method, which leads to the arrangement of cells in agglomerates (called spheroids) of various composition and sizes,[35] more accurate, organotypic culture systems have been obtained by culturing the cells in hydrogels that mimic the ECM, such as collagen gels or Matrigel.[33,36] Although such 3D systems are much closer to the pathological microenvironment than 2D ones, they completely rely on the use of very soft matrices based on animal-derived biomaterials (e.g. collagen, laminin, etc.), which suffer from large batch-to-batch variability and need particular handling care, thus making experimental reproducibility harder to achieve. In this scenario, PEG-based hydrogels[32,37-43] and cryogels[23,24,26] appear as powerful alternatives to conventional organotypic culture models for the production of reproducible tumor tissue equivalents.

In this work, we preliminarily investigated the potential of novel PEG-based semi-IPN cryogels, based on poly(ethylene glycol) diacrylate (PEGDA) and type I collagen, as tunable off-the-shelf platforms for 3D cancer cell research. Being the main component of the tumor interstitial ECM, we selected type I collagen as a secondary polymer for the creation of the semi-IPNs, so as to enhance the biomimetic features of the cryogels. Firstly, we verified the feasibility of synthesizing the semi-IPN cryogels by means of fast ultraviolet (UV) irradiation. While the synthesis of PEGDA cryogels is commonly obtained through the use of the ammonium persulfate/tetramethylethylenediamine (APS/TEMED) redox initiating system,[23,25,26] we recently reported the faster synthesis of PEGDA cryogels by means of UV exposure, showing that the PEGDA concentration has a significant effect on the

cryogel pore size and stiffness.[44] Here, we further tested whether the addition of low amounts of collagen (up to 1% w/v) to a fixed PEGDA concentration (10% w/v) could allow the formation of tunable semi-IPN cryogels. Three cryogel formulations (PEG1, PEG2 and PEG3), differing in their collagen content, were prepared and characterized to assess the effect of collagen on their pore structure, swelling capability, degradation rate and mechanical stiffness.

Then, we evaluated the ability of these off-the-shelf cryogels to sustain the long-term viability, growth and morphology of two pancreatic ductal adenocarcinoma (PDAC) cell populations having different growth properties, i.e. the Panc1 cancer parenchymal cells (CPCs) and their derived cancer stem cells (CSCs). The choice of these specific cell lines was based on our previously established 2D and 3D organotypic culture models, the latter resembling *in vivo* PDAC growth during malignant progression.[45] The effect of the semi-IPN cryogels on the growth and morphology of the two selected PDAC cell lines was evaluated up to 14 days of culture, by performing the Resazurin reduction assay along with fluorescence and colorimetric cell staining. Experimental results were then compared with those of our previously established 2D and 3D organotypic culture models,[45] as well as with those obtained by preliminarily suspending the cells in Matrigel right before seeding onto the cryogels. Considering that Matrigel recapitulates the basement membrane environment of epithelial structures[46] and affects the growth kinetics of PDAC cells,[45] this last set of experiments allowed us to evaluate whether the use of Matrigel, together with the semi-IPN cryogel platforms, could further boost the cell growth.

2. MATERIALS AND METHODS

2.1 Cryogel synthesis

Cryogels were synthesized from aqueous mixtures of low molecular weight poly(ethylene glycol) diacrylate (PEGDA 700 Da, Sigma Aldrich, Milan, Italy) and purified, acid soluble type I collagen, derived from calfskin via pepsin extraction (Symatese Biomateriaux, Chaponost, France).

As previously reported,[47-49] dry collagen flakes (2% w/v) were dispersed in distilled water by magnetic stirring for about 6 hours, under refrigerating conditions (temperature < 10 °C) in order to avoid collagen denaturation. A whitish, homogeneous collagen suspension was obtained. A given amount of the suspension was then added to and thoroughly mixed with an aqueous solution of PEGDA and

2,2'-Azobis (2-methyl-N-(2-hydroxyethyl) propionamide), commercially known as VA-086 (Wako Chemicals Europe, Neuss, Germany). Water-soluble VA-086 was used as a photoinitiator (at a concentration of 0.5% w/v) due to its well-known cytocompatibility.[50] The final PEGDA concentration in the mixture was 10% w/v, while the collagen concentration was either 0.1% or 1% w/v (Fig. 1A). Control PEGDA solutions devoid of collagen were also prepared.

The mixtures were then degassed via centrifugation (6,000 rpm, 10 min) to remove air bubbles, transferred into aluminum dishes (diameter 60 mm) and frozen on the shelf of a freeze-dryer (AdVantage Pro, VirTis), by refrigerating from +20 °C to -20 °C in 1 hour (freezing rate 0.66 °C/min) and then holding at -20 °C for an additional hour, to allow for uniform freezing (Fig. 1B). The frozen mixtures were rapidly taken out from the freeze-drier and exposed to UV irradiation (365 nm, 2 mW cm^{-2}) for 3 min to allow for PEGDA crosslinking (Fig. 1C). The so-obtained cryogels were finally thawed for 10-20 min at room temperature and washed in a large amount of distilled water overnight, for full swelling and leaching out of unreacted diffusible chemicals (Fig. 1D).

For each cryogel formulation, synthesis was performed in triplicate and here will be referred to as PEG1, PEG2 and PEG3 for collagen concentrations of 0, 0.1 and 1% w/v respectively. From each batch of synthesis, multiple samples were cut by means of a biopsy punch (diameter 6 mm) and used for further characterization (Fig. 1E).

2.2 Cryogel characterization

2.2.1 FT-IR spectroscopy

The chemical composition of the cryogels was assessed using a Perkin Elmer Spectrum One IR Spectrometer in ATR mode. Cryogel samples were air-dried in a ventilated oven at 30 °C for 3 hours, and then their absorption spectra were collected in the range 4000 cm^{-1} to 400 cm^{-1} with a resolution of 4 cm^{-1}, averaging over 64 scans. Air-dried collagen suspension was used as a reference for collagen.

2.2.2 Gelation yield

Immediately after the washing in distilled water, cryogel discs (n=5) were transferred to a ventilated oven at 30 °C for 3-4 hours, until a constant, dry weight was obtained (W_{dry}). Known the theoretical quantity of precursors (i.e. PEGDA and collagen) used in the reaction mixture to synthesize the different kinds of cryogels ($W_{precursor}$), the gelation yield (GY) was calculated as follows[51]:

$$GY = \frac{W_{dry}}{W_{precursor}} \times 100 \qquad \text{(Equation 1)}$$

2.2.3 Morphological analyses

The cryogel pore structure was visualized by means of confocal laser scanning microscopy (CLSM) and scanning electron microscopy (SEM).

For CLSM, hydrated cryogels were preliminarily grafted with acryloxyethyl thiocarbamoyl Rhodamine B (acryl-rhodamine B, Polysciences Europe), in order to take advantage of the fluorescent signal emitted by this molecule. In particular, cryogel samples were immersed in a solution containing acryl-rhodamine B at a final concentration of 0.1% w/v, and VA-086 (0.5% w/v). The cryogels were then exposed to UV irradiation for 3 min to graft the acryl-rhodamine B stain on the surface of their pore walls. After being abundantly washed with distilled water, hydrated samples were observed with a LSM 700 laser scanning confocal microscope (Zeiss).

For SEM analysis, swollen cryogel samples were preliminarily freeze-dried (to preserve their pore structure) and then observed with an EVO 40 scanning electron microscope (Zeiss) in a variable pressure mode.

Obtained micrographs from both CLSM and SEM observations were finally analyzed through the use of ImageJ software (National Institutes of Health, USA), to estimate the average pore size distribution of each cryogel type, over 100 pores.

2.2.4 Macropore volume

For highly porous materials such as cryogels, the water located inside large and interconnected pores can move freely, so that it can be removed by physical squeezing. The macropore volume (MV) fraction of the cryogels was roughly estimated by means of gravimetric measurements, as previously reported[51]:

$$MV = \frac{W_{swollen} - W_{squeezed}}{W_{swollen}} \times 100 \qquad \text{(Equation 2)}$$

In the above equation, $W_{swollen}$ and $W_{squeezed}$ are the weights of cryogels swollen in distilled water (n=5), before and after squeezing respectively.

2.2.5 Swelling measurements

Cryogel discs (n=5), weighing W_{dry} following desiccation in oven, were incubated in phosphate buffered saline (PBS, pH 7.4) at room temperature for 24 hours. Hydrated samples were then removed from the solution, gently tapped onto filter paper and weighed again to determine the fully swollen weight ($W_{swollen}$). The swelling capability was expressed as the mass swelling ratio (Q), calculated as follows:

$$Q = \frac{W_{swollen} - W_{dry}}{W_{dry}} \qquad \text{(Equation 3)}$$

The swelling kinetics of the cryogels was also assessed by recording their swelling over time, in particular after 15, 30, 60, 120 and 300 s of incubation in PBS. The swelling ratio at time t (Q_t) was calculated as described above, and expressed as percentage of the full swelling ratio Q attained after a 24-hour incubation. Kinetic results for each cryogel type were averaged over 3 independent measurements.

2.2.6 Degradation analysis

The cryogel degradation due to prolonged incubation at physiological conditions was assessed gravimetrically. Briefly, dehydrated cryogel specimens of known weight were submerged in PBS and placed in an incubator at 37 °C and 5% CO_2 humidified air, to mimic *in vitro* culture conditions. After 7, 14, 21 and 28 days, cryogels (n=5 for each time point) were transferred to a ventilated oven at 30 °C for complete drying. The ratio between the sample weight at time t and its initial weight was then used to evaluate the weight loss percentage at a given time interval.

2.2.7 Mechanical measurements

The mechanical properties of the cryogels were investigated by means of unconfined compression tests. Cryogel discs (n=3) were preliminarily hydrated in PBS at room temperature for 24 h. The matrices were then mounted on a Z1.0 TH testing machine (Zwick Roell), equipped with a 10 N load cell and a bath chamber. Swollen samples were compressed at room temperature at a displacement rate of 0.01 mm/s, until 50% of their initial height. The slope of the linear elastic region detected in the stress-strain curves at low strain values (in the range 0-2%) was then calculated to estimate the compressive modulus (at time 0).

Further compression tests were then performed following prolonged incubation of the cryogels in PBS at 37 °C (i.e. after 7, 14, 21 and 28 days), in order to evaluate the potential decrease of mechanical stiffness resulting from degradation under *in vitro* conditions. The compressive modulus measured at time t (n=3 for each time point) was compared with that measured at time 0.

2.3 3D cancer cell culture

2.3.1 Cell lines

The human pancreatic adenocarcinoma cell line Panc1 (parenchymal cells, CPCs) were grown in adherent conditions in RPMI 1640 supplemented with 10% FBS, 2

mM glutamine, and 50 µg/ml gentamicin sulfate (Gibco, Life Technologies) at 37 °C with 5% CO_2. CSCs were selected from Panc1 (the Parental line) as previously described[52] and identified by their ability to form anchorage independent colonies and by their overexpression of common CSC markers.[52] CSCs were cultured in DMEM/F-12 without glucose (US Biological Life Sciences) supplemented with 1g/l glucose, B27 serum substitute (Gibco, Life Technologies), 1 µg/ml Fungizone (Gibco, Life Technologies), 1% penicillin/streptomycin (Gibco, Life Technologies), 5 µg/ml heparin (Sigma Aldrich), 20 ng/ml EGF (epidermal growth factor, Peprotech), and 20 ng/ml FGF (fibroblast growth factor, Peprotech) at 37 °C with 5% CO_2.

2.3.2 3D culture and growth of Panc1 CPCs and CSCs on cryogels

For cell culture cryogels, preliminarily sterilized by immersion in ethanol (70% v/v) for 2 hours, were placed into the wells of a 24-well plate. Cells were washed once with 1×PBS, detached with 0.25% Trypsin − 0.53 mM EDTA solution, counted by using a Neubauer hemocytometer chamber and 15 X 10^3 cells of each cell line were re-suspended in 20 µl of the corresponding growth medium (prepared as described above), either in the absence or presence of 4mg/ml Matrigel. Each 20 µl drop of cell suspension was deposited on the upper surface of each of the three types of cryogels (n=3 for each cryogel type). Scaffolds with cells were incubated at 37 °C and 5% CO_2 for 30 min to let the drop be absorbed and to allow the cells to adhere on and within the scaffold. After which, 200 µl of cell growth medium was added to each well to completely cover the scaffold. Cells were cultured for two weeks by refreshing the growth medium every 2-3 days. In order to measure cell viability over time, Resazurin (Immunological Sciences) reduction assay was performed at several time points (0, 5, 7, 12 and 14 days) by directly incubating the scaffolds with 10 µl stock Resazurin (44µM) in 200 µl medium and measuring fluorescence (Ex=560 nm, Em=590 nm) with the Cary Eclipse Plate Reader (Varian) after 3 hours. A sample of each cryogel type (PEG1, PEG2, PEG3) without cells and having injected or not with only Matrigel was used as a negative control.

2.3.3 F-actin staining analysis

At the 14th day of growth, cell colonization inside the 3D cryogels was evaluated by staining F-actin of embedded cells with TRITC-conjugated Phalloidin. Cryogels were washed 2X with cold PBS and fixed with 3.7% ice-cold paraformaldehyde/PBS for 30 min. Fixed cryogels were washed with ice-cold PBS, permeabilized with 0.1%

TRITON X-100 for 30 min, rinsed with PBS and incubated with Phalloidin-TRITC (Molecular Probes) 1:5000 in PBS for 45 min. Scaffolds were mounted onto glass slides and fluorescence was visualized with a Nikon TE 2000S epifluorescence microscope equipped with a MicroMax 512BFT CCD camera (Princeton Instruments) using a Nikon lamp shutter with a mercury short arc photo optic HBO 103 W/2 lamp for excitation (OSRAM).

2.3.4 Histological analysis

Samples were embedded in Technovit 8100 kit (Electron Microscopy Sciences). First, they were fixed in a 4% paraformaldehyde solution in 0.1 M PBS pH 7.4 at 4 °C for 3 h. After rinsing in PBS, pieces were incubated overnight, at 4 °C, in PBS with 6.8% added sucrose, and then dehydrated with increasing acetone, also at 4 °C. Samples were subsequently subjected to infiltration by incubating them in a Technovit 8100 monomer for 6 h at 4 °C. Finally, samples were embedded with an ice-cold solution of 15:1 infiltrating solution. Polymerization was performed on an ice bed for 3 h. Semi-thin sections (2-mm thick) were cut with glass knives using an LKB Ultratome and mounted on microscope slides, coated with polylysine. Semi-thin sections were stained with toluidine blue to assess the general morphology of the cells.

2.4 Statistical analysis

All data were expressed as mean ± standard error (SE), unless otherwise noted. Statistical significance was determined by using ANOVA and Fisher's PLSD tests, and differences were considered to be statistically significant when p value < 0.05.

3. RESULTS

3.1 Synthesis of PEGDA/collagen semi-IPN cryogels by means of UV irradiation

Semi-IPN cryogels based on PEGDA and type I collagen were synthesized via UV irradiation of frozen aqueous mixtures of the two polymers. In particular, three polymer mixtures, namely PEG1, PEG2 and PEG3 having a collagen concentration of 0, 0.1 and 1% w/v respectively, were prepared. PEG1 formulation, devoid of collagen, was used as a reference, while composite PEG2 and PEG3 formulations allowed to assess the feasibility of the semi-IPN cryogels and to verify the potential effect of the collagen concentration on the cryogel properties.

FTIR analysis was first utilized to verify the presence of collagen in the blended cryogel formulations. As well known, protein marker bands are amides I, II and III,

which are respectively ascribable to the C=O stretching mode (Amide I, 1670-1620 cm^{-1}), the N-H stretching mode (Amide II, 1570-1530 cm^{-1}) and the C-N stretching mode (Amide III, 1270-1230 cm^{-1}) of the peptide bonds.[53] The collagen spectrum (in the wavenumber range 1850-700 cm^{-1}) was dominated by the amide I, II and III bands, respectively found at about 1631 cm^{-1}, 1545 cm^{-1} and 1236 cm^{-1} (Fig. 2A). Conversely, the pure PEGDA cryogel (PEG1) showed characteristic absorption bands at 1730 cm^{-1} and 1096 cm^{-1}, attributable to C=O and C-O-C vibrational modes, respectively (Fig. 2A).[9,25]

When analyzing the spectra of PEG2 and PEG3 (Fig. 2B), amide I and II bands were clearly visible for both samples, together with the typical peaks of the PEGDA cryogel at 1730 and 1096 cm^{-1}. This confirmed the presence of both components in the blended formulations. Compared to PEG1, PEG2 and PEG3 cryogels also showed a more pronounced absorption band at about 1243-1283 cm^{-1}, likely due to the overlapped IR signals of the C-O asymmetric bending of PEG1[9,25] and the amide III band of collagen. Additional signal overlapping in the amide I region, due to the C=O stretching of both the PEGDA network (at 1629-1648 cm^{-1}, PEG1)[25] and the protein, likely contributed to the shift of the amide I band position (from about 1631 to 1654 cm^{-1}) found for PEG2 and PEG3 samples, with respect to pure collagen. However, this shift may also indicate some changes in the secondary structure of the protein, due to the different amide I contributions ascribed to triple helical (at 1631 cm^{-1}) and α-helical structures (at 1658 cm^{-1}).[49] In this regard, it is also interesting to observe that, in spite of having a higher collagen concentration, PEG3 sample showed a lower and more symmetric amide I band compared to PEG2, as well as a reduced amide II band. In general, changes in the amide I absorption might be ascribed to different protein chain conformations, also in relation to the supramolecular organization, with a higher band intensity attributed to increased structural order.[54] On the contrary, a lower intensity of the amide II band may be due to hydrogen abstraction or structural scission of N-H bonds, which occur in the presence of free radicals.[55,56] Based on the FTIR spectra, we thus inferred that the cryogel synthesis could induce a certain damage of the collagen structure, which was more evident at higher protein amounts, as a result of: a) structural deformations, taking place upon the physical interpenetration with the PEGDA network in the cryo-concentrated regions, with the cryo-concentration being enhanced at higher protein amounts; b) photochemical scissions, ascribed to the free radical exposure during UV crosslinking and favored by

the locally increased cryo-concentration. Additional structural alterations of collagen during the freeze-thaw cycle, particularly due to the expansion of the intra-fibrillar space by ice formation,[57] may also occur in PEG2 and PEG3 samples and contribute to the shape and intensity of the respective amide I bands, compared to pure collagen. Overall, qualitative FTIR analysis demonstrated that, although not taking part to the chemical crosslinking reaction, collagen was successfully retained in the PEGDA network, thus leading to the formation of semi-IPN cryogels. However, the analysis also suggested that partial collagen degradation could be concurrently achieved, especially at higher protein contents.

The gelation yield (GY) was then evaluated to assess the efficiency of the UV-induced cryo-gelation process (Table 1). Notably, the GY was found to increase for increasing collagen content ($p < 0.0001$), being about 82%, 88% and 90% for PEG1, PEG2 and PEG3 cryogels, respectively. The additional presence of collagen in the blended samples thus favored the gelation process, likely due to the enhanced cryo-concentration effect.

3.2 Effect of collagen concentration on the cryogel properties

With the ultimate aim of using the proposed PEGDA/collagen semi-IPN cryogels as potential matrices for 3D cancer cell research, we assessed whether the collagen concentration could affect some key properties of the cryogels important for cell culture, respectively the porosity, the hydration capability, the degradation rate and the mechanical stiffness.

Confocal (Fig. 3A) and SEM (Fig. 3B) microscopy, performed on hydrated and freeze-dried samples respectively, confirmed that the cryogels had a highly homogeneous porous structure with interconnecting pores and smooth pore walls. Notably, quantitative image analysis highlighted that the average pore size and the pore size distribution tended to decrease and get narrow as the collagen concentration was increased (Fig. 3C, 3D, 3E). Average pore dimensions of 58 ± 17 μm, 37 ± 11 μm and 24 ± 8 μm (mean ± SD) were estimated for PEG1, PEG2 and PEG3 cryogels, respectively. Such an effect of collagen on the pore size was likely ascribed to the increased viscosity of the polymer mixtures yielded for increasing amounts of collagen, which are expected to limit the diffusion of water molecules during freezing, thus hampering ice crystal growth and, consequently, the achievable pore

size.[58] However, all cryogels showed an average pore size suitable for cell culture applications.

Consistently with the pore dimensions, the macropore volume (MV) of the cryogels was also significantly affected by the collagen concentration (Table 1; p<0.0001). The MV, which was about 70% for both PEG1 and PEG2 cryogels (p=0.22), was significantly reduced down to 60% for the PEG3 specimens (PEG1 vs. PEG3 and PEG2 vs. PEG3, p<0.0001).

The porous and highly interconnected structure of the cryogels was also demonstrated by their swelling/hydration kinetics (Supplementary Fig. S1). As expected, all of the samples displayed a very fast hydration, with PEG1, PEG2 and PEG3 reaching approximately the 99%, 94% and 75% of their full swelling within 1 min. In accordance with the effect of collagen concentration on the pore size, the swelling rate tended to decrease as the collagen content was increased.

With regard to the full swelling (Table 1), it is worth noting that the amount of water uptake generally depends on both physical (e.g. porosity) and chemical (e.g. crosslink density) structural parameters.[59,60] While porosity tends to enhance the swelling by capillary water retention, with higher retention achieved by smaller pore sizes, the crosslink density strongly limits the swelling, due to the elastic retraction exerted by the crosslinking nodes on the polymer chains.[59,60] Here, we found that the full swelling of the cryogels decreased as the collagen amount was increased (p<0.0001). This result was thus likely attributable to a higher crosslink density of the cryogels attained in the presence of collagen, due to the enhanced cryo-concentration.

Upon prolonged incubation in PBS at 37 °C, we then found that all of the cryogels denoted a modest although significant (p<0.0001) weight loss, which reached, over 28 days, values of about 10%, 20% and 25% for PEG1, PEG2 and PEG3 samples, respectively (Fig. 4A). It is well known that PEG-based networks, such as PEG1 cryogels, undergo a slow degradation at physiological conditions, due to hydrolysis.[61] The additional presence of collagen to form semi-IPN cryogels appeared to accelerate the overall weight loss, especially in the first 1-2 weeks of PBS incubation. In particular, at day 7 PEG3 samples displayed a significantly higher degradation compared to PEG1 and PEG2 ones (PEG1 vs. PEG3, p=0.0077; PEG2 vs. PEG3, p=0.02), both of which showed, at the same time point, comparable weight losses (PEG1 vs. PEG2, p=0.70). However, starting from day 14, detected differences between PEG2 and PEG3 were no longer relevant. Notably, these findings were

consistent with those of the FTIR analysis, which indicated a higher extent of collagen degradation achieved in PEG3 cryogels, compared to PEG2 ones. It is thus conceivable that the more extensively degraded collagen in PEG3 samples could be released more rapidly under physiological conditions, leading to a faster weight loss in the first 7 days.

In parallel to degradation experiments, mechanical compression tests were also performed on the hydrated cryogels to evaluate their stiffness along the 28-day incubation period. Following compression down to 50% deformation without breaking, cryogels could indeed rapidly recover their original size, so that their stiffness could be monitored over time. As shown in Fig. 4B, the average compressive elastic modulus of the cryogels was initially about 51, 49 and 62 kPa for PEG1, PEG2 and PEG3 samples, respectively. Although the differences were not significant, this trend appeared in rough agreement with the swelling results, thus further suggesting a higher crosslink density attained in the presence of collagen. Interestingly, the average modulus of the cryogels did not decrease significantly along the study. A slight reduction of the stiffness was only found for the collagen-containing samples (PEG2 and PEG3), while PEG1 cryogels were highly stable.

3.3 Growth of Panc1 CPC and CSC cells in the cryogels

In order to verify the potential of the semi-IPN cryogels as tunable platforms for cancer cell research, we investigated their ability to entrap and permit the growth of a highly aggressive parenchymal PDAC cell line (CPC), Panc1, and their derived CSCs. We decided to study PDAC as a tumor model, as its high malignancy is mainly due to the presence of a highly fibrotic, collagen I-rich stroma that creates a tumor-supportive environment promoting tumor growth, early invasion and therapy resistance.[45,62,63] In this respect, we have already established standard PDAC organotypic cultures of Panc1 parenchymal cells (CPCs) and CSC cells growing on different ECMs (from a Matrigel-rich ECM to an ever more collagen I-rich ECM) that recapitulate the malignant stromal activation observed in the *in vivo* disease.[45,64,65] By using this organotypic platforms we have demonstrated that: (1) Resazurin, a soluble dye that is reduced to highly fluorescent Resorufin in proportion to cell metabolic activity, is a reliable indicator of CPC and CSC cell numbers and growth within the 3D ECM[45]; (2) CPCs and CSCs have completely different 3D growth kinetics which are, depending on the ECM substrate, completely reversed compared to those

observed in 2D[45,52]; (3) the growth matrix composition affects PDAC cell growth morphology and kinetics.[45] Indeed, on Matrigel-rich ECM, the CSCs grew almost four-fold faster than CPCs but as ECMs became ever more enriched of type I collagen, the CPCs' and CSCs' growth rate slowed down and became approximately equal, with only a slight gain of growth of the CPCs over the CSCs.[45]

To verify whether the CPCs and CSCs could colonize the three types of cryogels, eventually expanding into tumor masses, and to characterize their growth dynamics, we embedded the two cell lines into the three types of cryogels and monitored cell viability over time up to 14 days, by using the Resazurin-based growth assay (Fig. 5).

We found that CPCs grew significantly faster than CSCs for up to 14 days in both PEG1 (with no collagen) and PEG2 (1 mg/ml, 0.1%). This accelerated growth of the CPCs compared to CSCs reproduces the typical CPC and CSC kinetic growth found in 2D.[52] However, the growth rates of CPCs and CSCs were comparable when cells were cultured in PEG3, which had increased collagen concentration (10 mg/ml, 1%) and restricted pore sizes. Indeed, we found that, when grown in PEG3, CSCs grew significantly faster than in PEG1 and PEG2 and expanded with the same growth kinetic as CPCs (Fig. 5A).

We hypothesized that the higher CSC growth in PEG3, compared to PEG1 and PEG2, could be due either to pro-adhesion signals provided by the presence of collagen I into PEG3 or to the restricted pore sizes of PEG3. However, when CSCs and CPCs were seeded into porous scaffolds entirely based on collagen I (30 mg/ml)[47,48] and having a similar pore size as PEG1 (i.e. about 60-70 μm) (Supplementary Methods and Fig. S2), we found that the two cell lines reproduced the same growth dynamics as observed when they were grown in PEG3 (RFU for CPCs 474.28 ± 57.74 vs. CSCs 504.19 ± 18.20 at 5 days) (Supplementary Fig. S3). This suggests that indeed it is the presence of a sufficiently high quantity of collagen that is responsible for the increased CSC growth. Moreover, the growth pattern exhibited by the CPCs and CSCs expanding in PEG3 reproduces the growth kinetics detected for CPCs and CSCs cultured on collagen I-enriched organotypic cultures[45] indicating that, among the three cryogel types, PEG3 is the most suitable to mimic the CSC and CPC growth rates as *in vivo* and permit the analysis of the cell behavior.

The growth dynamics of the two tumor cell lines within the different cryogel types were also confirmed by immunofluorescence experiments, in which we visualized cell growth and morphology by staining their F-actin cytoskeleton with Rhodamine

Phalloidine after 14 days of cell growth. As shown in Fig. 5B, we found that both CPCs and CSCs colonized the scaffolds and expanded after two weeks as already shown by the Resazurin test. No qualitative changes in morphology and/or organization for the two cell lines seeded within the different cryogels were detected. Cell infiltration and growth in the bulk of the scaffolds at 14 days were also confirmed by histological analysis, which showed cells uniformly distributed in both the outer (external) and the inner scaffold layers (Fig. 5C).

As Matrigel is widely used in cancer culture models to simulate the environment of a basement membrane of epithelial structures[46] and we reported that CSCs grow faster than CPCs on Matrigel-rich organotypic cultures,[45] we additionally explored the potential contribution of Matrigel on the CPCs and the CSCs long-term growth ability in the different cryogel types. For this, CPC and CSC growth rates were monitored with the Resazurin-based growth assay at 5, 7, 12 and 14 days after having seeded cells, pre-embedded in Matrigel drops, inside each type of cryogel (Fig. 6A).

We found that Matrigel pre-embedding favored CSCs over CPCs growth in the different cryogel types, but only up to 7 days as, surprisingly, after a week of culture both cell lines stopped growing. We also found that cell pre-inclusion in Matrigel drops *per se* strongly hindered cell growth of both cell lines in the cryogels, compared to the same cell growth observed without Matrigel pre-inclusion (Fig. 5A). This hampered growth ability was also confirmed by immunofluorescence microscopy of Phalloidin-stained cells at the end of each experiment (Fig. 6B) and suggests that Matrigel pre-embedding could have a negative effect on either the initial infiltration of the seeded cells inside the cryogels, or on their migration throughout the cryogels and/or on their subsequent long-term cellular expansion.

To determine if cell pre-inclusion in Matrigel could, indeed, affect cell seeding efficiency or cell infiltration, distribution and growth into the deeper layers of the cryogels, the cryogels were fixed at 24 hours after cell seeding, sectioned and stained with toluidine blue. The individual stained sections were imaged and the densities and distributions of cells within the individual sections were then analyzed. As shown in Fig. 6C, a limited amount of either CPCs or CSCs infiltrated the three types of cryogels, with most cells appearing along the seeding edge on the external cryogels' layers, and very low cell densities occurred with increasing depth into the center of the cryogels (inner layers). This poor cell infiltration demonstrates that, while cryogels represent a powerful and reproducible tool for hosting CPCs and CSCs,

permitting their expansion and monitoring over long time periods (with PEG3 likely being the most suitable for cell growth), cells pre-embedding in animal derived-matrices such as Matrigel, before their seeding into the scaffolds, interferes with their efficient inclusion into the scaffolds and the possibility to derive 3D spheroids and eventually organoids.

4. DISCUSSION

In this work, we prepared PEGDA/collagen semi-IPN cryogels by means of UV irradiation and tested their potential as tunable and reproducible platforms for cancer cell research. As a proof of concept, we assessed their ability to host the long-term growth of two PDAC cell lines and to allow the monitoring of the cell behavior over time.

Firstly, we started by investigating the feasibility of the synthesis of the PEGDA/collagen semi-IPN cryogels. The strong hydrophilic nature of PEG (and its derivatives) is known to induce the precipitation of various proteins in solution, including collagen.[66] With reference to the synthesis of blended systems made of PEGDA and type I collagen, several studies have reported the preliminary modification of collagen or its gelatin derivative with (meth)acrylated groups, in order to obtain, upon cross-linking, a hybrid polymer network composed of PEGDA and protein.[25,67] The use of cell-adhesive peptides, instead of the entire proteins, is another widely explored method to develop hybrid PEGDA networks.[10,11] A further approach involves the sequential synthesis of IPNs, where a PEGDA hydrogel is crosslinked in the presence of a previously formed collagen network.[7] Very few studies have then been reported on the possibility to form PEGDA/collagen semi-IPNs, where these are obtained by directly crosslinking PEGDA by UV exposure, in the presence of un-crosslinked collagen molecules.[3-5] In particular, a quite low weight ratio between collagen and PEGDA in the initial mixture (which appears translucent or whitish opaque) is reported to lead, upon UV crosslinking, to homogeneous semi-IPN hydrogels with cell-adhesive properties.[3-5]

In this work, we investigated whether UV irradiation could be used to produce PEGDA/collagen semi-IPN cryogels as well. UV and high-energy irradiation have been commonly reported for the synthesis of cryogels based on various polysaccharides, such as cellulose, dextran and alginate.[21,68,69] Recently, we have shown that pure PEGDA cryogels can also be obtained via UV irradiation, as a faster

alternative to the classical APS/TEMED activated cryo-crosslinking.[44] In that study, we found that the PEGDA concentration significantly affects the swelling, the stiffness and the porosity of the UV-irradiated cryogels.[44] Here, we used a fixed PEGDA concentration, equal to 10% w/v,[5] and then incorporated the PEGDA solution with variable amounts of collagen, to assess the yet unexplored effect of collagen on the cryogel properties. Blended PEG2 and PEG3 formulations had collagen/PEGDA weight ratios equal to 1/100 and 1/10, respectively, in accordance with those previously reported for the preparation of semi-IPN hydrogels.[3-5]

Although local changes in the polymer and protein distributions were likely to occur upon freezing, we expected that the low collagen amount (compared to the PEGDA) could be physically entrapped within the PEGDA network upon UV crosslinking. Moreover, we hypothesized that the presence of collagen in the semi-liquid zones among ice crystals, in addition to the PEGDA, could lead to a higher cryo-concentration effect, thus increasing the effectiveness of gelation/crosslinking, for a given UV exposure time. As expected, FTIR analysis (Fig. 2A and 2B) confirmed that collagen was retained in the semi-IPN cryogels, while the enhanced gelation yield (Table 1) attained for higher collagen contents suggested a higher gelation/crosslinking of the semi-IPNs. In this respect, collagen may not only lead to an increased cryo-concentration effect, but also establish physical entanglements or other types of physical interactions with the PEGDA network, thus contributing to the overall crosslinking of the semi-IPNs. However, as suggested by FTIR spectra, the interpenetration with the PEGDA network upon UV cryo-crosslinking, especially at higher protein amounts, could also cause partial protein damage, likely ascribable to concurrent structural/mechanical deformations of the collagen fibrils as well as photochemical degradation. Therefore, our results indicate that the synthesis of PEGDA/collagen semi-IPN cryogels can be performed via UV irradiation, provided that sufficiently low protein amounts are used, both to avoid inhomogeneous protein distributions in the starting blend and to limit the extent of collagen damage upon cryo-gelation.

We then assessed the effect of collagen on important cryogel properties, starting from their porosity. Especially for 3D cell culture, cryogel macropores are advantageous to enhance the size of the bio-constructs that can be generated *in vitro*. The modulation of the cryogel porosity, achieved by controlling the freezing and the gelation processes, also allows tuning other macroscopic properties of the cryogels (e.g.

density of cell-interactive sites, water uptake, degradation rate) that may regulate the cellular behavior. Notably, the presence of collagen was found to affect significantly the pore size distribution of the cryogels. Smaller pore sizes were indeed obtained for increasing collagen amounts (Fig. 3). This was likely ascribed to the formation of smaller ice crystal upon freezing, due to the increased viscosity of the PEGDA/collagen liquid blends. Consequently, the macropore volume was also reduced with the collagen content (Table 1).

Swelling data, with diminished water uptakes for increasing collagen amounts, seemed to further confirm what suggested by the gelation yield, i.e. the crosslinking tended to improve as the collagen concentration was increased (Table 1). However, prolonged incubation of the cryogels at physiological conditions (Fig. 4A) evidenced an accelerated gravimetric degradation of the semi-IPN samples over the pure PEGDA ones, especially in the first 7-14 days. This provided hints that the enhanced crosslinking achieved for the semi-IPN cryogels was likely attributable to a higher number of physically crosslinked molecules, which were then released in the incubating medium after several days. Moreover, the partial degradation of collagen within the blended cryogels (as suggested by the FTIR spectra) could also explain the faster weight loss of these samples. In this regard, PEG3 cryogels were the ones showing the most rapid degradation in the first 7 days, in agreement with the presence in PEG3 of a more extensively degraded collagen.

Interestingly, the compressive stiffness of the cryogels, which was not significantly affected by the collagen content (at least for the values under investigation), was practically unchanged over the entire 28-day incubation period (Fig. 4B). In general, the rigidity of substrates used for 3D cancer cell culture plays a key role in regulating the growth and invasiveness of cancer cells,[43,70,71] as well as the tumor resistance to chemotherapeutics.[27] It is worth noting that the average stiffness of the cryogels described in this work ($\approx$50 kPa) is roughly comparable with the optimal values recently suggested for the culture of bone ($\approx$50 kPa)[70] and prostate cancer tissues ($\approx$75 kPa).[23] The achieved stiffness values were also consistent with those obtained in our previous work on UV-irradiated PEGDA cryogels having the same PEGDA concentration (10% w/v).[44] In that study, we showed that the compressive modulus of the cryogels is significantly tuned by the PEGDA concentration, with values down to 10 kPa and up to 150 kPa, for a PEGDA concentration of 5% w/v and 15% w/v, respectively.[44] Therefore, while the collagen concentration does not seem to affect the

cryogel stiffness, we envisage the intriguing possibility to modulate the stiffness of the semi-IPN cryogels by changing the PEGDA concentration. This would allow optimizing the cryogel platforms, by tailoring their mechanical properties to those of the specific cancer tissue(s) being addressed.

Finally, to verify 'tout court' the suitability of the cryogels as substrates for cancer cell research, we tested their ability to host the growth of two PDAC cell lines, i.e. the highly aggressive parenchymal Panc1 CPCs and their derived CSCs. While several studies have recently reported the use of *in situ* forming PEG-based hydrogels to study the PDAC cell fate in 3D,[41-43] to the best of our knowledge this is the first study attempting to use off-the-shelf PEGDA-based cryogels for PDAC cell culture.

In spite of the simplicity of our semi-IPN cryogel platforms, we interestingly found that all of the cryogels supported CPCs and CSCs infiltration and expansion, up to 14 days of culture (Fig. 5). Moreover, the cellular growth rate was significantly affected by the collagen content. In particular, when grown in PEG1 cryogels (devoid of collagen), both CPCs and CSCs reproduced their growth pattern previously observed in 2D culture conditions. Conversely, PEG3 cryogels (i.e. those having the highest collagen concentration, 1% w/v) allowed the proliferation of both cell lines with growth kinetics similar to those previously reported in collagen I-enriched organotypic 3D cultures.[45] Furthermore, although Matrigel is known to facilitate the growth of several tumor cells, including PDAC cells,[45,46] we found here that the cellular pre-embedding in Matrigel, before their seeding into the cryogels, hindered an efficient cell infiltration and proliferation. This limitation, together with problems related to cost, inhomogeneity and low reproducibility of Matrigel-like matrices, indicates that the proposed semi-IPN cryogel platforms (especially PEG3) hold potential to be used as tunable and reproducible alternatives to organotypic cultures based on ECM-derived matrices. However, since the ECM contains various components useful to recapitulate the tumor microenvironment, we envisage that the additional functionalization of the semi-IPN cryogels with physiomimetic ECM-derived peptides, along with a proper tuning of their mechanical properties, might be the most promising approach to create optimized bioengineered platforms for 3D cancer cell research.

5. CONCLUSION

Novel semi-IPN cryogels based on PEGDA and type I collagen, having variable collagen content (0, 0.1 and 1% w/v for PEG1, PEG2 and PEG3 cryogels, respectively), were produced by means of UV irradiation. Experimental findings suggested that higher collagen amounts induced the formation of cryogels with enhanced crosslink density, although partial collagen degradation might be concurrently achieved. Collagen was found to have a deep impact on the cryogel porosity, with smaller pore sizes attained for increasing protein amounts. All of the cryogels showed a modest weight loss up to 28 days of incubation in PBS at 37 °C, while being mechanically stable over the entire incubation period. The potential of the semi-IPN cryogels to be used as tunable, off-the-shelf platforms for 3D cancer cell culture was then explored by analyzing the growth of two PDAC cell lines within them. Interestingly, the growth kinetics of PDAC parenchymal cells and CSCs growing either in the PEG1 cryogels (without collagen) or in the PEG3 cryogels (with 1% w/v collagen) reproduced the growth pattern previously observed when the two cell lines were cultured respectively in 2D conditions (i.e. without collagen) or in collagen I-enriched organotypic 3D cultures. Moreover, our results also showed that cellular pre-embedding in Matrigel, right before seeding into the cryogels, interferes with an efficient cell infiltration and migration into the center of the cryogels, while also hindering the long-term cell proliferation. Considering that Matrigel provides key signaling molecules to cancer cells, this finding suggests that the best protocol to increase the ECM-mimicking properties of the cryogels would likely require their functionalization with ECM-derived peptides. These engineered PEGDA/collagen semi-IPN cryogels could thus represent standardized, ready-to-use matrices, alternative to less reproducible organotypic cultures.

ACKNOWLEDGEMENTS

REFERENCES

1. Myung D, Waters D, Wiseman M, Duhamel P-E, Noolandi J, Ta CN, Frank CW. Progress in the development of interpenetrating polymer network hydrogels. Polym Adv Technol 2008;19(6):647-657. https://doi.org/10.1002/pat.1134

2. Kutty JK, Cho E, Lee JS, Vyavahare NR, Webb K. The effect of hyaluronic acid incorporation on fibroblast spreading and proliferation within PEG-diacrylate based semi-interpenetrating networks. Biomaterials 2007;28:4928-4938. https://doi.org/10.1016/j.biomaterials.2007.08.007

3. Hwang NS, Varghese S, Li H, Elisseeff J. Regulation of osteogenic and chondrogenic differentiation of mesenchymal stem cells in PEG-ECM hydrogels. Cell Tissue Res 2011;344(3):499-509. https://doi.org/10.1007/s00441-011-1153-2

4. Chan BK, Wippich CC, Wu C-J, Sivasankar PM, Schmidt G. Robust and semi-interpenetrating hydrogels from poly(ethylene glycol) and collagen for elastomeric tissue scaffolds. Macromol Biosci 2012;12:1490-1501. https://doi.org/10.1002/mabi.201200234

5. Madaghiele M, Marotta F, Demitri C, Montagna F, Maffezzoli A, Sannino A. Development of semi- and grafted interpenetrating polymer networks based on poly(ethylene glycol) diacrylate and collagen. J Appl Biomater Funct Mater 2014;12(3):183-192. https://doi.org/10.5301/jabfm.5000187

6. Skaalure SC, Dimson SO, Pennington AM, Bryant SJ. Semi-interpenetrating networks of hyaluronic acid in degradable PEG hydrogels for cartilage tissue engineering. Acta Biomater 2014;10(8): 3409-3420. https://doi.org/10.1016/j.actbio.2014.04.013

7. Munoz-Pinto DJ, Jimenez-Vergara AC, Gharat TP, Hahn MS. Characterization of sequential collagen-poly(ethylene glycol) diacrylate interpenetrating networks and initial assessment of their potential for vascular tissue engineering. Biomaterials 2015;40:32-42. https://doi.org/10.1016/j.biomaterials.2014.10.051

8. Hong S, Sycks D, Chan HF, Lin S, Lopez GP, Guilak F, Leong KW, Zhao X. 3D printing of highly stretchable and tough hydrogels into complex, cellularized structures. Adv Mater 2015;27:4035-4040. https://doi.org/10.1002/adma.201501099

9. Punyamoonwongsa P, Klayya S, Sajomsang W, Kunyanee C, Aueviriyavit S. Silk sericin semi-interpenetrating network hydrogels based on PEG-diacrylate for wound healing treatment. Int J Polym Sci 2019: 4740765. https://doi.org/10.1155/2019/4740765

10. Mann BK, Gobin AS, Tsai AT, Schmedlen RH, West JL. Smooth muscle cell growth in photopolymerized hydrogels with cell adhesive and proteolytically degradable domains: synthetic ECM analogs for tissue engineering. Biomaterials 2001;22(22):3045-3051. https://doi.org/10.1016/S0142-9612(01)00051-5

11. Singh SP, Schwartz MP, Lee JY, Fairbanks BD, Anseth KS. A peptide functionalized poly(ethylene glycol) (PEG) hydrogel for investigating the influence of biochemical and biophysical matrix properties on tumor cell migration. Biomater Sci 2014;2(7): 1024-1034. https://doi.org/10.1039/C4BM00022F

12. Wieland JA, Houchin-Ray TL, Shea LD. Non-viral vector delivery from PEG-hyaluronic acid hydrogels. J Control Release 2007;120(3):233-241. https://doi.org/10.1016/j.jconrel.2007.04.015

13. Freudenberg U, Hermann A, Welzel PB, Stirl K, Schwarz SC, Grimmer M, Zieris A, Panyanuwat W, Zschoche S, Meinhold D, Storch A, Werner C. A star-PEG-heparin hydrogel platform to aid cell replacement therapies for neuroregenerative diseases. Biomaterials 2009;30:5049-5060. https://doi.org/10.1016/j.biomaterials.2009.06.002

14. Tong X, Yang F. Engineering interpenetrating network hydrogels as biomimetic cell niche with independently tunable biochemical and mechanical properties. Biomaterials 2014, 35:1807-1815. https://doi.org/10.1016/j.biomaterials.2013.11.064

15. Lee S, Tong X, Yang F. The effects of varying poly(ethylene glycol) hydrogel crosslinking density and the crosslinking mechanism on protein accumulation in three-dimensional hydrogels. Acta Biomater 2014;10(10):4167-4174. https://doi.org/10.1016/j.actbio.2014.05.023

16. Annabi N, Nichol JW, Zhong X, Ji C, Koshy S, Khademhosseini A, Dehghani F. Controlling the Porosity and Microarchitecture of Hydrogels for Tissue Engineering. Tissue Eng Part B 2010;16(4):371-383. https://doi.org/10.1089/ten.teb.2009.0639

17. Keskar V, Marion NW, Mao JJ, Gemeinhart RA. *In Vitro* Evaluation of Macroporous Hydrogels to Facilitate Stem Cell Infiltration, Growth, and Mineralization. Tissue Eng Part A 2009;15(7):1695-1707. https://doi.org/10.1089/ten.tea.2008.0238

18. Welzel PB, Grimmer M, Renneberg C, Naujox L, Zschoche S, Freudenberg U, Werner C. Macroporous starPEG-heparin cryogels. Biomacromolecules 2012;13: 2349-2358. https://doi.org/10.1021/bm300605s

19. Henderson TMA, Ladewig K, Haylock DN, McLean KN, O'Connor AJ. Cryogels for biomedical applications. J Mater Chem B 2013;1:2682-2695. https://doi.org/10.1039/C3TB20280A

20. Hwang Y, Sangaj N, Varghese S. Interconnected Macroporous Poly(Ethylene Glycol) Cryogels as a Cell Scaffold for Cartilage Tissue Engineering. Tissue Eng A 2010;16(10):3033-3041. https://doi.org/10.1089/ten.TEA.2010.0045

21. Bencherif SA, Sands RW, Battha D, Arany P, Verbeke CS, Edwards DA, Mooney DJ. Injectable preformed scaffolds with shape-memory properties. PNAS 2012;109:19590-19595. https://doi.org/10.1073/pnas.1211516109

22. Oelschlaeger C, Bossler F, Willenbacher N. Synthesis, Structural and Micromechanical Properties of 3D Hyaluronic Acid-Based Cryogel Scaffolds. Biomacromolecules 2016;17(2):580-589. https://doi.org/10.1021/acs.biomac.5b01529

23. Göppert B, Sollich T, Abaffy P, Cecilia A, Heckmann J, Neeb A, Bäcker A, Baumbach T, Gruhl FJ, Cato ACB. Superporous Poly(ethylene glycol) Diacrylate Cryogel with a Defined Elastic Modulus for Prostate Cancer Cell Research. Small 2016;12(29):3985-3994. https://doi.org/10.1002/smll.201600683

24. Zhang G, Song X, Mei J, Ye G, Wang L, Yu L, Xing MMQ, Qiu X. A simple 3D cryogel co-culture system used to study the role of CAFs in EMT of MDA-MB-231 cells. RSC Adv 2017;7:17208-17216. https://doi.org/10.1039/C6RA28721B

25. Shrimali P, Peter M, Singh A, Dalal N, Dakave S, Chiplunkar SV, Tayalia P. Efficient in situ gene delivery via PEG diacrylate matrices. Biomater Sci 2018;6:3241-3250. https://doi.org/10.1039/C8BM00916C

26. Singh A, Tayalia P. Three-dimensional cryogel matrix for spheroid formation and anti-cancer drug screening. J Biomed Mater Res A 2020;108(2):365-376. https://doi.org/10.1002/jbm.a.36822

27. Rice AJ, Cortes E, Lachowski D, Cheung BCH, Karim SA, Morton JP, del Río Hernández A. Matrix stiffness induces epithelial–mesenchymal transition and promotes chemoresistance in pancreatic cancer cells. Oncogenesis 2017;6(7): e352. https://doi.org/10.1038/oncsis.2017.54

28. Voskoglou-Nomikos T, Pater JL, Seymour L. Clinical predictive value of the in vitro cell line, human xenograft, and mouse allograft preclinical cancer models. Clin Cancer Res 2003;9(11):4227-4239.

29. Lovitt CJ, Shelper TB, Avery VM. Advanced cell culture techniques for cancer drug discovery. Biology 2014;3(2):345-367. https://doi.org/10.3390/biology3020345

30. Dumont N, Liu B, Defilippis RA, Chang H, Rabban JT, Karnezis AN, Tjoe JA, Marx J, Parvin B, Tlsty TD. Breast fibroblasts modulate early dissemination, tumorigenesis, and metastasis through alteration of extracellular matrix characteristics. Neoplasia 2013;15(3):249-262. https://doi.org/10.1593/neo.121950

31. Balhouse B, Ivey J, Verbridge SS. Engineered microenvironments for cancer study, in: T. Baldacchini (Ed.), Three-dimensional microfabrication using two-photon polymerization, pp. 417-446, Elsevier (2016).

32. Lin CC, Korc M. Designer hydrogels: Shedding light on the physical chemistry of the pancreatic cancer microenvironment. Cancer Letters 2018;436:22-27. https://doi.org/10.1016/j.canlet.2018.08.008

33. Zeeberg K, Cardone RA, Greco MR, Saccomanno M, Nohr-Nielsen A, Alves F, Pedersen SF, Reshkin SJ. Assessment of different 3D culture systems to study tumor phenotype and chemosensitivity in pancreatic ductal adenocarcinoma. Int J Oncol 2016;49(1):243-252. https://doi.org/10.3892/ijo.2016.3513

34. Pradhan S, Hassani I, Clary JM, Lipke EA. Polymeric biomaterials for in vitro cancer tissue engineering and drug testing applications. Tissue Eng Part B 2016;22(6):470-484. https://doi.org/10.1089/ten.TEB.2015.0567

35. Foty R. A simple hanging drop cell culture protocol for generation of 3D spheroids. J Vis Exp 2011;51. https://doi.org/10.3791/2720

36. Kim JB. Three-dimensional tissue culture models in cancer biology. Semin Cancer Biol 2005;15:365-377. https://doi.org/10.1016/j.semcancer.2005.05.002

37. DelNero P, Song YH, Fischbach C. Microengineered tumor models: insights & opportunities from a physical sciences-oncology perspective. Biomed Microdevices 2013;15(4):583-593. https://doi.org/10.1007/s10544-013-9763-y

38. Hutmacher DW, Loessner D, Rizzi S, Kaplan DL, Mooney DJ, Clements JA. Can tissue engineering concepts advance tumor biology research? Trends Biotechnol 2010;28(3):125-133. https://doi.org/10.1016/j.tibtech.2009.12.001

39. Worthington P, Pochan DJ, Langhans SA. Peptide hydrogels – Versatile matrices for 3D cell culture in cancer medicine. Frontiers in Oncology 2015;5:92. https://doi.org/10.3389/fonc.2015.00092

40. Brancato V, Garziano A, Gioiella F, Urciuolo F, Imparato G, Panzetta V, Fusco S, Netti PA. 3D is not enough: Building up a cell instructive microenvironment for tumoral stroma microtissues. Acta Biomater 2017;47: 8-13. https://doi.org/10.1016/j.actbio.2016.10.007

41. Ki CS, Lin T-Y, Korc M, Lin C-C. Thiol-ene hydrogels as desmoplasia-mimetic matrices for modeling pancreatic cancer cell growth, invasion, and drug resistance. Biomaterials 2014;35(36):9668-9677. https://doi.org/10.1016/j.biomaterials.2014.08.014

42. Raza A, Ki CS, Lin C-C. The influence of matrix properties on growth and morphogenesis of human pancreatic ductal epithelial cells in 3D. Biomaterials 2013;34(21):5117-5127. https://doi.org/10.1016/j.biomaterials.2013.03.086

43. Liu H-Y, Korc M, Lin C-C. Biomimetic and enzyme-responsive dynamic hydrogels for studying cell-matrix interactions in pancreatic ductal

24

adenocarcinoma. Biomaterials 2018;160:24-36. https://doi.org/10.1016/j.biomaterials.2018.01.012

44. Madaghiele M, Salvatore L, Demitri C, Sannino A. Fast synthesis of poly(ethylene glycol) diacrylate cryogels via UV irradiation. Mater Letter 2018;218:305-308. https://doi.org/10.1016/j.matlet.2018.02.048

45. Biondani G, Zeeberg K, Greco MR, Cannone S, Dando I, Dalla Pozza E, Mastrodonato M, Forciniti S, Casavola V, Palmieri M, Reshkin SJ, Cardone RA. Extracellular Matrix composition modulates PDAC parenchymal and stem cell plasticity and behavior through the secretome. FEBS J 2018;285:2104-2124. https://doi.org/10.1111/febs.14471

46. Lv D, Hu Z, Lu L, Lu H, Xu X. Three-dimensional cell culture: A powerful tool in tumor research and drug discovery. Oncol Lett 2017;14:6999-7010. https://doi.org/10.3892/ol.2017.7134

47. Salvatore L, Madaghiele M, Parisi C, Gatti F, Sannino A. Crosslinking of micropatterned collagen-based nerve guides to modulate the expected half-life. J Biomed Mater Res A 2014;102:4406-4414. https://doi.org/10.1002/jbm.a.35124

48. Monaco G, Cholas R, Salvatore L, Madaghiele M, Sannino A. Sterilization of collagen scaffolds designed for peripheral nerve regeneration: Effect on microstructure, degradation and cellular colonization. Mat Sci Eng C 2017;71: 335-344. https://doi.org/10.1016/j.msec.2016.10.030

49. Terzi A, Storelli E, Bettini S, Sibillano T, Altamura D, Salvatore L, Madaghiele M, Romano A, Siliqi D, Ladisa M, De Caro L, Quattrini A, Valli L, Sannino A, Giannini C. Effects of processing on structural, mechanical and biological properties of collagen-based substrates for regenerative medicine. Sci Rep 2018;8:1429. https://doi.org/10.1038/s41598-018-19786-0

50. Rouillard AD, Berglund CM, Lee JY, Polacheck WJ, Tsui Y, Bonassar LJ, Kirby BJ. Methods for Photocrosslinking Alginate Hydrogel Scaffolds with High Cell Viability. Tissue Eng C 2011;17(2):173-179. https://doi.org/10.1089/ten.tec.2009.0582

51. Dispinar T, Van Camp W, De Cock LJ, De Geest BG, Du Prez FE. Redox responsive degradable PEG cryogels as potential cell scaffolds in tissue engineering. Macromol Biosci 2012;12:383-394. https://doi.org/10.1002/mabi.201100396

52. Dalla Pozza E, Dando I, Biondani G, Brandi J, Costanzo C, Zoratti E, Fassan M, Boschi F, Melisi D, Cecconi D, Scupoli MT, Scarpa A, Palmieri M. Pancreatic ductal adenocarcinoma cell lines display a plastic ability to bidirectionally convert into cancer stem cells. Int J Oncol 2014;46:1099-1108. https://doi.org/10.3892/ijo.2014.2796

53. Belbachir K, Noreen R, Gouspillou G, Petibois C. Collagen types analysis and differentiation by FTIR spectroscopy. Anal Bioanal Chem 2009;395:829-837. https://doi.org/10.1007/s00216-009-3019-y

54. de Campos Vidal B, Mello MLS. Collagen type I amide I band infrared spectroscopy. Micron 2011;42:283-289. https://doi.org/10.1016/j.micron.2010.09.010

55. Kamińska A, Sionkowska A. Effect of UV radiation on the infrared spectra of collagen. Polym Degr Stab 1996;51:19-26. https://doi.org/10.1016/0141-3910(95)00159-X

56. Rabotyagova OS, Cebe P, Kaplan DL. Collagen structural hierarchy and susceptibility to degradation by ultraviolet radiation. Mater Sci Eng C 2008;28(8):1420-1429. https://doi.org/10.1016/j.msec.2008.03.012

57. Ozcelikkale A, Han B. Thermal Destabilization of Collagen Matrix Hierarchical Structure by Freeze/Thaw. PLoS ONE 2016;11(1):e0146660. https://doi.org/10.1371/journal.pone.0146660

58. Madaghiele M, Sannino A, Yannas IV, Spector M. Collagen-based matrices with axially oriented pores. J Biomed Mater Res A 2008;85(3):757-767. https://doi.org/10.1002/jbm.a.31517

59. Sannino A, Netti PA, Madaghiele M, Coccoli V, Luciani A, Maffezzoli A, Nicolais L. Synthesis and characterization of macroporous poly(ethylene glycol)-based hydrogels for tissue engineering applications. J Biomed Mater Res A 2006;79:229-236. https://doi.org/10.1002/jbm.a.30780

60. Flory PJ. Principles of Polymer Chemistry. Cornell University Press, Ithaca NY, (1953).

61. Browning MB, Cereceres SN, Luong PT, Cosgriff-Hernandez EM. Determination of the in vivo degradation mechanism of PEGDA hydrogels. J Biomed Mater Res A 2014;102(12):4244-4251. https://doi.org/10.1002/jbm.a.35096

62. Ware MJ, Keshishian V, Law JJ, Ho JC, Favela CA, Rees P, Smith B, Mohammad S, Hwang RF, Rajapakshe K, Coarfa C, Huang S, Edwards DP, Corr SJ, Godin B, Curley SA. Generation of an in vitro 3D PDAC stroma rich spheroid model. Biomaterials 2016;108:129-142. https://doi.org/10.1016/j.biomaterials.2016.08.041

63. Erkan M, Reiser-Erkan C, Michalski CW, Kleeff J. Tumor microenvironment and progression of pancreatic cancer. Exp Oncol 2010;32(3):128-131.

64. Puls TJ, Tan X, Whittington CF, Voytik-Harbin SL. 3D collagen fibrillar microstructure guides pancreatic cancer cell phenotype and serves as a critical design parameter for phenotypic models of EMT. PLoS One 2017;12:e0188870. https://doi.org/10.1371/journal.pone.0188870

65. Shields MA, Dangi-Garimella S, Redig AJ, Munshi HG. Biochemical role of the collagen-rich tumour microenvironment in pancreatic cancer progression. Biochem J 2012;441:541-552. https://doi.org/10.1042/BJ20111240

66. Sim S-L, He T, Tscheliessnig A, Mueller M, Tan RBH, Jungbauer A. Protein precipitation by polyethylene glycol: a generalized model based on hydrodynamic radius. J Biotechnol 2012;157:315-319. https://doi.org/10.1016/j.jbiotec.2011.09.028

67. Gaudet ID, Shreiber ID. Characterization of methacrylated type I collagen as a dynamic, photoactive hydrogel. Biointerphases 2012;7:25. https://doi.org/10.1007/s13758-012-0025-y

68. Petrov P, Petrova E, Tsvetanov CB. UV-assisted synthesis of super-macroporous polymer hydrogels. Polymer 2009;50(5):1118-1123. https://doi.org/10.1016/j.polymer.2008.12.039

69. Georgiev GL, Trzebicka B, Kostova B, Petrov PD. Super-macroporous dextran cryogels via UV-induced crosslinking: synthesis and characterization. Polym Int 2017;66(9):1306-1311. https://doi.org/10.1002/pi.5386

70. Jabbari E, Sarvestani SK, Daneshian L, Moeinzadeh S. Optimum 3D Matrix Stiffness for Maintenance of Cancer Stem Cells Is Dependent on Tissue Origin of Cancer Cells. PLoS ONE 2015;10(7):e0132377. https://doi.org/10.1371/journal.pone.0132377

71. Haage A, Schneider IC. Cellular contractility and extracellular matrix stiffness regulate matrix metalloproteinase activity in pancreatic cancer cells. FASEB J 2014;28(8):3589-3599. https://doi.org/10.1096/fj.13-245613

CAPTIONS TO TABLES AND FIGURES

Table 1. Gelation yield (GY), macropore volume (MV) and swelling ratio (Q) of the cryogels. Reported data were averaged over 5 measurements and expressed as mean ± standard error (SE). [a]Significant difference from PEG1; [b]Significant difference from PEG2

Figure 1. Schematic representation of cryogel synthesis. (A) Aqueous polymer mixtures having 10% w/v PEGDA, different concentrations of collagen and 0.5% w/v VA-086 are prepared and degassed; (B) mixtures are frozen from +20 °C to -20 °C in 1 hour and then kept 1 hour at -20 °C to permit ice crystal formation; (C) frozen mixtures are immediately exposed to UV irradiation (365 nm, 2 mW/cm^2) for 3 min; (D) crosslinked cryogels are thawed for 10-20 min at room temperature and then abundantly washed in distilled water. A photogragh of a cryogel sample in the hydrated state is reported in (E).

Figure 2. Cryogel composition by means of FTIR analysis. (A) Comparison between the spectra of pure collagen and pure PEGDA cryogel (PEG1), with the highlight of their characteristic peaks; (B) comparison among the spectra of collagen and the tested cryogels (PEG1, PEG2 and PEG3), showing the presence of both collagen and PEG in the blended formulations (PEG2 and PEG3).

Figure 3. Cryogel microstructure and quantitative analysis of pore size. (A) Confocal microscopy images showing hydrated cryogels stained with acryl-rhodamine B (scale bar 100 μm) and (B) SEM micrographs of freeze-dried cryogels (500X, scale bar 15 μm). Pore diameter distribution of PEG1 (C), PEG2 (D) and PEG3 (E) cryogels estimated by means of ImageJ, and their average pore size (F). Error bars in (F) represent the standard error (SE).

Figure 4. Cryogel degradation and stiffness upon prolonged incubation in PBS at 37 °C. (A) Weight loss of PEG1 (blue), PEG2 (red) and PEG3 (green) cryogels (n=5) and (B) corresponding compressive elastic modulus (n=3). Error bars represent the standard error (SE).

Figure 5. Growth of Panc1 CPC and CSC cells in the cryogels. (A) Cell viability of CPCs and CSCs growing in PEG1, PEG2 and PEG3 for 14 days. Fold change in cell growth was calculated by measuring CPC and CSC cell viability with the Resazurin assay. CPC and CSC growth values were normalized to their respective 5-day growth in PEG1. Data are mean ± SE of 4 independent experiments, *$p<0.05$ refers to CPC growth compared to CSC growth into each cryogel, #$p<0.05$ and ##$p<0.01$ refers to CSC growth among the different cryogels. (B) Immunofluorescence images of cells growing in PEG1, PEG2 and PEG3 after 14 days. The cells were stained for actin by using phalloidin-TRITC and imaged with a epifluorescence microscope with a 10X objective. (C) Cell images and distribution of PEG1, PEG2 and PEG3 seeded with CPCs and CSC, sectioned and stained with Toluidine Blue. The inner layers of the scaffolds show a similar cell density and distribution to that of the more external layers (bar 100μm).

Figure 6. Growth of Matrigel-embedded Panc1 CPC and CSC cells in the cryogels. (A) Cell viability of Matrigel-embedded CPCs and CSCs in PEG1, PEG2 and PEG3

for 14 days. Cell pre-inclusion in Matrigel (4mg/ml) favored CSC growth compared to CPCs only up to one week of culture, after which cell growth for both cell lines diminished in all cryogels. Data are mean ± SE of 5 independent experiments. *$p<0.05$ and **$p<0.01$ refer to CPC growth compared to CSC growth into the same cryogel type. (B) Immunofluorescence analysis of CPCs and CSCs pre-embedded in Matrigel drops before their seeding into the cryogels. Seeded cells were imaged by staining their F-actin with Phalloidin-Rhodamine at 14 growth day (bar 100μm). (C) Cell images and distribution of CPCs and CSCs pre-embedded in Matrigel drops, seeded into the cryogels and stained with Toluidine Blue. The external layers of the cryogels show a high cell density along the seeded edge of the scaffolds while the inner layers of the cryogels show minimal cell presence (bar 100μm).

Table 1. Gelation yield (GY), macropore volume (MV) and swelling ratio (Q) of the cryogels.

Reported data were averaged over 5 measurements and expressed as mean ± standard error (SE).

Sample	GY (%)	MV (%)	Q (g/g)
PEG1	82.0 ± 0.8	70.3 ± 0.9	10.3 ± 0.1
PEG2	88.5 ± 0.4^{a}	71.7 ± 1.0	9.8 ± 0.3
PEG3	$90.9 \pm 0.5^{a,b}$	$59.7 \pm 0.4^{a,b}$	$8.5 \pm 0.1^{a,b}$

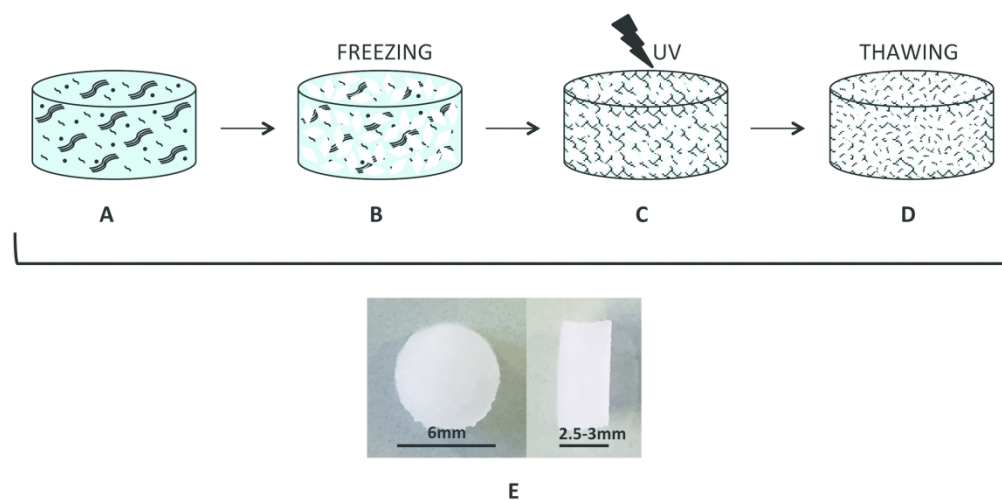[a]Significant difference from PEG1; [b]Significant difference from PEG2

Figure 1. Schematic representation of cryogel synthesis. (A) Aqueous polymer mixtures having 10% w/v PEGDA, different concentrations of collagen and 0.5% w/v VA-086 are prepared and degassed; (B) mixtures are frozen from +20 °C to -20 °C in 1 hour and then kept 1 hour at -20 °C to permit ice crystal formation; (C) frozen mixtures are immediately exposed to UV irradiation (365 nm, 2 mW/cm2) for 3 min; (D) crosslinked cryogels are thawed for 10-20 min at room temperature and then abundantly washed in distilled water. A photogragh of a cryogel sample in the hydrated state is reported in (E).
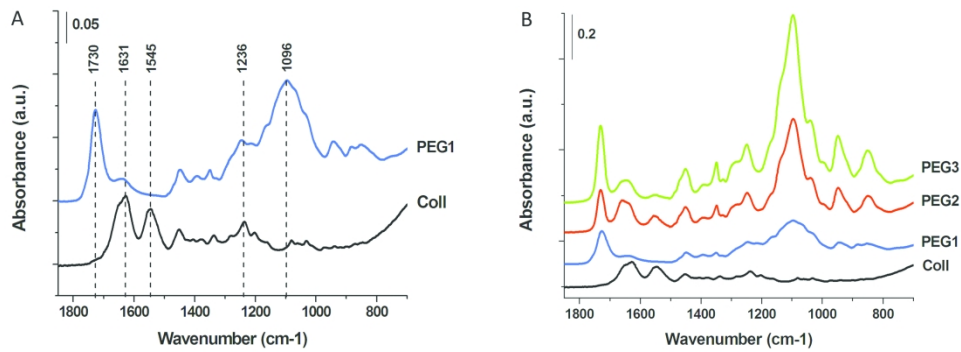
116x57mm (600 x 600 DPI)

Figure 2. Cryogel composition by means of FTIR analysis. (A) Comparison between the spectra of pure collagen and pure PEGDA cryogel (PEG1), with the highlight of their characteristic peaks; (B) comparison among the spectra of collagen and the tested cryogels (PEG1, PEG2 and PEG3), showing the presence of both collagen and PEG in the blended formulations (PEG2 and PEG3).

157x57mm (600 x 600 DPI)
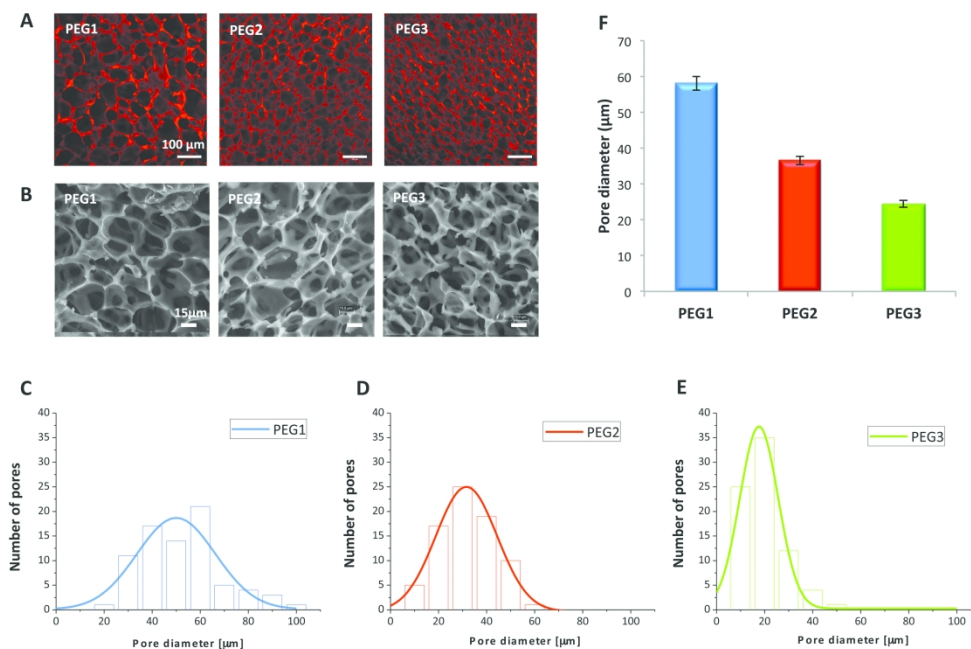
Cryogel microstructure and quantitative analysis of pore size. (A) Confocal microscopy images showing hydrated cryogels stained with acryl-rhodamine B (scale bar 100 µm) and (B) SEM micrographs of freeze-dried cryogels (500X, scale bar 15 µm). Pore diameter distribution of PEG1 (C), PEG2 (D) and PEG3 (E) cryogels estimated by means of ImageJ, and their average pore size (F). Error bars in (F) represent the standard error (SE).
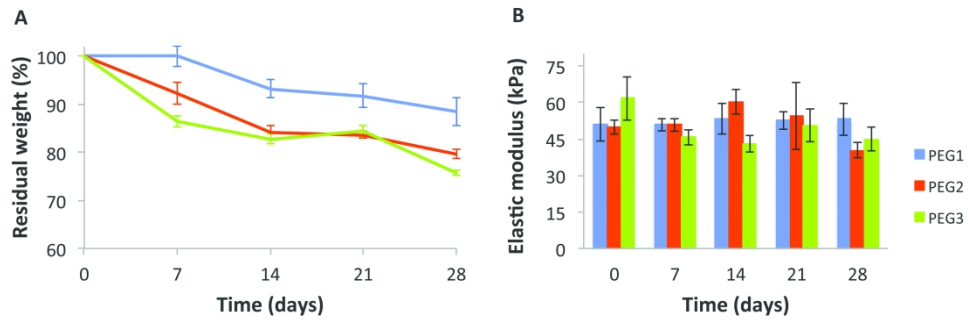
159x104mm (600 x 600 DPI)

Figure 4. Cryogel degradation and stiffness upon prolonged incubation in PBS at 37 °C. (A) Weight loss of PEG1 (blue), PEG2 (red) and PEG3 (green) cryogels (n=5) and (B) corresponding compressive elastic modulus (n=3). Error bars represent the standard error (SE).
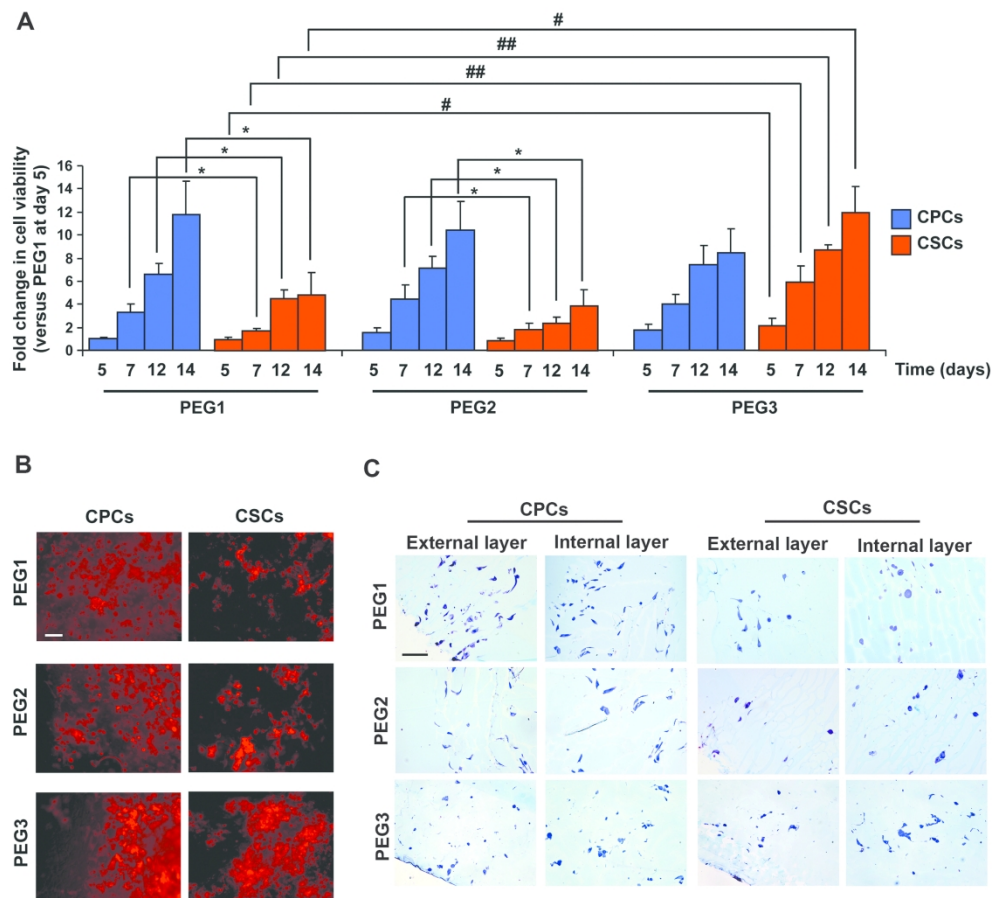
160x54mm (600 x 600 DPI)

Figure 5. Growth of Panc1 CPC and CSC cells in the cryogels. (A) Cell viability of CPCs and CSCs growing in PEG1, PEG2 and PEG3 for 14 days. Fold change in cell growth was calculated by measuring CPC and CSC cell viability with the Resazurin assay. CPC and CSC growth values were normalized to their respective 5-day growth in PEG1. Data are mean ± SE of 4 independent experiments, *$p < 0.05$ refers to CPC growth compared to CSC growth into each cryogel, #$p < 0.05$ and ##$p < 0.01$ refers to CSC growth among the different cryogels. (B) Immunofluorescence images of cells growing in PEG1, PEG2 and PEG3 after 14 days. The cells were stained for actin by using phalloidin-TRITC and imaged with a epifluorescence microscope with a 10X objective. (C) Cell images and distribution of PEG1, PEG2 and PEG3 seeded with CPCs and CSC, sectioned and stained with Toluidine Blue. The inner layers of the scaffolds show a similar cell density and distribution to that of the more external layers (bar 100μm).
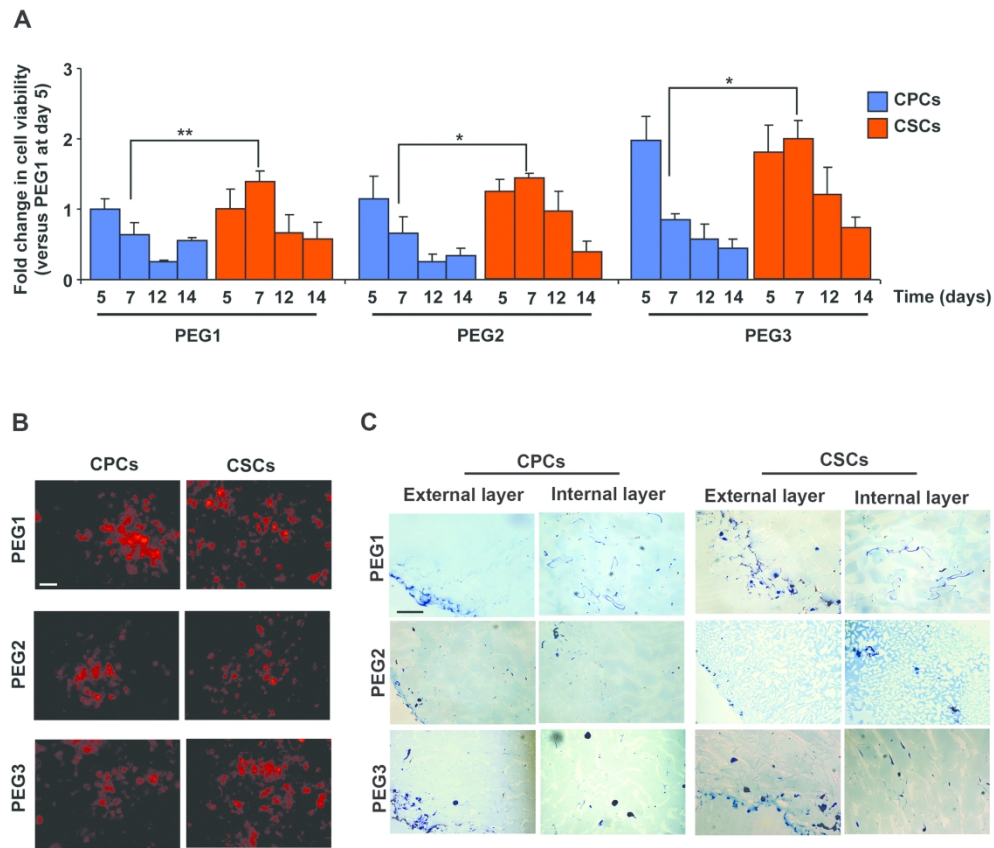
114x105mm (600 x 600 DPI)

Figure 6. Growth of Matrigel-embedded Panc1 CPC and CSC cells in the cryogels. (A) Cell viability of Matrigel-embedded CPCs and CSCs in PEG1, PEG2 and PEG3 for 14 days. Cell pre-inclusion in Matrigel (4mg/ml) favored CSC growth compared to CPCs only up to one week of culture, after which cell growth for both cell lines diminished in all cryogels. Data are mean ± SE of 5 independent experiments. *p<0.05 and **p<0.01 refer to CPC growth compared to CSC growth into the same cryogel type. (B) Immunofluorescence analysis of CPCs and CSCs pre-embedded in Matrigel drops before their seeding into the cryogels. Seeded cells were imaged by staining their F-actin with Phalloidin-Rhodamine at 14 growth day (bar 100μm). (C) Cell images and distribution of CPCs and CSCs pre-embedded in Matrigel drops, seeded into the cryogels and stained with Toluidine Blue. The external layers of the cryogels show a high cell density along the seeded edge of the scaffolds while the inner layers of the cryogels show minimal cell presence (bar 100μm).

114x100mm (600 x 600 DPI)